Computers in Biology and Medicine 110 (2019) 186–195

Contents lists available at ScienceDirect

Computers in Biology and Medicine

journal homepage: www.elsevier.com/locate/compbiomed

An open-source plugin for OpenSim® to model the non-linear behaviour of dense connective tissues of the human knee at variable strain rates

Arnab Sikidar[a], Dinesh Kalyanasundaram[a,b,*]

[a] Centre for Biomedical Engineering, Indian Institute of Technology Delhi, New Delhi, 110016, India
[b] Department of Biomedical Engineering, All India Institute of Medical Sciences, New Delhi, 110029, India

ARTICLE INFO

Keywords:
Dense connective tissues (DCTs)
OpenSim®
Non-linear strain rate (NLSR)
Viscoelasticity
Musculoskeletal knee models

ABSTRACT

The force-length characteristics of dense connective tissues (DCTs) vary non-linearly as a function of strain rate. However, there is no class of OpenSim® available to incorporate the effect of strain rate into the OpenSim® model. In this work, a new plugin for OpenSim® was developed to incorporate the non-linear strain rate behaviour of dense connective tissues (DCTs) of the human knee. Experimental force-length plots from the literature were used to extract the shape factor, scale factor, the coefficient of viscosity and elastic stiffness corresponding to specific strain rates. A new class object termed as *NonLinearLigament* was formulated using a customized plugin based on a structural constitutive model. A test platform was created to evaluate the force-length patterns at multiple strain rates ranging from 0.0001 s^{-1} to 100 s^{-1} for the DCT bundles. Knee kinematics of 25 DCT bundles were subjected to forward simulation at various strain rates. To understand the significance, the force-length characteristics of each of the DCTs were simulated as a function of strain rate for both existing *Ligament* class of OpenSim® and the proposed *NonLinearLigament* class. In the proposed ligament class, higher forces were observed with an increase of strain rate in DCTs. Existing *Ligament* class in OpenSim® was devoid of any changes at different strain rates. In summary, the developed plugin takes into account the short term viscoelastic behaviour of DCTs and hence, would help in accurate modelling of tissue behaviour specifically for dynamic situations.

1. Background

Dense connective tissues (DCTs) including ligaments, tendons (dense regular connective tissue) and joint capsules (dense irregular connective tissue) are soft tissues in the knee joint [1]. DCTs are cardinal for the range of motion of the joint construct, and hence, an abnormality in these tissues induce the risk of immobility and permanent disability [2]. A ligament tear is one of the most common injuries sustained in these joints and requires conservative treatment or surgical reconstruction [3–5]. Due to the high rate of injuries in ligaments during dynamic activities, it is imperative to comprehend the force-length characteristics at varying strain rates. However, there exists merely a handful number of studies on varying strain rates of DCTs of the knee [6–8]. These studies correspond to a specific strain rate while the day-to-day physical activities encompass a wide range of strain rates on the knee [9]. Studies also suggest that the stress developed in a DCT is a non-linear function of strain rate [8,10]. Bonner et al. studied the tensile properties of the lateral collateral ligament (LCL) of porcine samples at strain rates ranging from 0.01 to 100 s^{-1} and concluded that there is a significant variation of tensile characteristics as a function of strain rate [11]. Hence, the strain rate effect is an essential feature of a DCT.

While physical experimentations of DCTs are imperative to the understanding of real-life behaviour, there are several constraints in carrying out such experiments for specific strain rate corresponding to every scenario. At this juncture, musculoskeletal modelling is an intuitive approach to study the effect of strain rate. Musculoskeletal modelling via rigid body mechanics or soft tissue mechanics are solved either finite elemental method (FEM) [7,12,13] or discrete elemental techniques [14–17]. FEM addresses highly complex inputs and provides quite an accurate solution. However, FEM based approaches suffer from the convergence of the solution and often demands high infrastructural costs of computation and time. On the other hand, discrete element techniques are quicker and highly recommended for studies where the joint stresses are redundant [18]. In order to accurately model soft tissue mechanics, the inclusion of inherent properties of the soft tissue is paramount to achieve results closer to the real-life situations [19]. OpenSim®, an open source musculoskeletal platform provides a

* Corresponding author. Centre for Biomedical Engineering, Indian Institute of Technology Delhi, New Delhi, 110016, India.
E-mail addresses: dineshk@cbme.iitd.ac.in, dineshk.iitdelhi@gmail.com (D. Kalyanasundaram).

https://doi.org/10.1016/j.compbiomed.2019.05.021
Received 18 March 2019; Received in revised form 27 May 2019; Accepted 29 May 2019

reasonably easy computation of kinematic and kinetic parameters including displacement, strain, velocity, acceleration, the range of motion etc., as well as joint reaction forces, tissue forces and moment arm using forward and inverse dynamics. In the past, Xu et al. followed by Schmitz et al. developed a lower extremity model in OpenSim® with 10 DCT bundles and 18 DCT bundles of the knee joint, respectively [16,20]. In both the articles, the two research groups defined DCTs with linear force-length characteristics. The authors of the current work had extended the above-mentioned knee model by incorporating 7 additional DCT bundles and identified *differential intra-bundle strain* as one of the failure defining parameters [21]. In all the three musculoskeletal models, the force-length characteristics were linear and were independent of the strain rate. However, in reality, the strain-rate (referred to as the short-term viscoelastic property) affects the force-length characteristics [22]. Koga and Muneta concluded that the injury time frame for ACL during dynamic activities ranges between 10 and 40 m s [23]. Therefore, to understand injury mechanics and simulate them, it is imperative to incorporate the strain-rate dependency of DCTs.

In summary, the non-linear strain rate (NLSR) behaviour of DCTs was incorporated via a custom plugin for OpenSim® musculoskeletal platform in this work. A graphical user interface (GUI) was developed in MATLAB® using De Vita and Slaughter's structural model [10,24]. The GUI was used to estimate the material parameters described in De Vita and Slaughter's model for the 20 DCT bundles (corresponding to nine ligaments) of knee joint from the experimental data. The remaining five DCT bundles were assumed to be similar in force-length characteristics as that of the menisco-femoral ligament. The material parameters were used to define the property of the DCT bundles along with maximum isometric force, resting length, failure strain and strain rate. The simulation was carried out to calculate the force-extension behaviour of the bundles at strain rates starting from 0.0001 s^{-1} to 100 s^{-1}. The DCT bundles modelled in this work were simulated under flexion, internal rotation, external rotation, adduction and abduction in the time frame of 10 and 40 m s.

2. Methods

2.1. Structural model for DCTs

De Vita and Slaughter's structural hyper-elastic model addresses the influence of strain rate on the force-length characteristics of the anterior cruciate ligament (ACL) [10]. Equation (1) shows the constitutive equation proposed by Pioletti et al. describing the first Piola-Kirchhoff stress tensor P. It was derived based on the assumption that the viscous potential $W_v(C, \dot{C})$ accounts for the energy dissipation. The formulation for $\boldsymbol{P}$ is

$$\boldsymbol{P} = -p\boldsymbol{G}^{-T} + 2\boldsymbol{G}.\left(\frac{\partial W_e(C)}{\partial C} + \frac{\partial W_v(C,\dot{C})}{\partial \dot{C}}\right) \tag{1}$$

where, the indeterminate pressure imposing the incompressibility assumption is given by p, the right Cauchy-Green deformation tensor is represented by $\boldsymbol{G}$, the elastic potential is given by $W_e(C)$, the material time derivative is indicated by C, and the dot product between vectors is represented by ".". The mean axial direction of the collagen fibres are assumed to be parallel to the direction of loading (E_z). Hence, a probability density function representing the fiber orientation is defined as $R(m) = \delta(m - E_z)$, where δ represents Dirac delta function and m indicates the direction coefficients of the collagen fiber. The elastic and viscous stresses of the fibers have been defined based on Kelvin–Voight-type viscoelastic constitutive behaviour as per reference [25]. Therefore, the Piola-Kirchhoff stress P_{zZ} is given by Ref. [10],

$$P_{zZ} = -p\lambda^{-1} + \sigma_e(\lambda) + \sigma_v(\lambda, \dot{\lambda}) \tag{2}$$

where, σ_e and σ_v are the elastic and viscous stresses developed in the collagen fiber. The values of these stresses are given by

$$\sigma_e(\lambda) = \int_1^{\lambda} R(\lambda_s)\bar{\sigma}_e\left(\frac{\lambda}{\lambda_s}\right)d\lambda_s; \quad \bar{\sigma}_e(\lambda) = K\ln\lambda \tag{2a}$$

$$\sigma_v(\lambda) = \int_1^{\lambda} R(\lambda_s)\bar{\sigma}_v\left(\frac{\lambda}{\lambda_s}, \frac{\dot{\lambda}}{\lambda_s}\right)d\lambda_s; \quad \bar{\sigma}_v(\lambda_r, \dot{\lambda}_r) = \eta\frac{D}{Dt}(\ln\lambda_r) \tag{2b}$$

where, $\bar{\sigma}_e$ and $\bar{\sigma}_v$ are the elastic and viscous stresses developed in each collagen fiber; $R(\lambda_s)$ is the probability density function describing the density of fibers that become active under a stretch λ_s; λ_r represents the stretch ratio between λ and λ_s; K and η are the elastic stiffness and the coefficient of viscosity of the fibers respectively. The term $\frac{D}{Dt}$ denotes the material time derivative. An assumption of traction-free boundary condition was made by De Vita et al. implicating the pressure term to be zero, i.e. $p = 0$. Therefore, Equation (2) can be expressed as.

$$P_{zZ} = \int_1^{\lambda} R(\lambda_s)\left\{K\ln\frac{\lambda}{\lambda_s} + \eta\frac{D}{Dt}\left(\ln\frac{\lambda}{\lambda_s}\right)\right\}d\lambda_s \tag{3}$$

Previous literature suggests that Weibull [10,24], Beta [26], and Gamma [27,28] distribution functions were implemented to model the uncrimping stretch of the collagen fibres. In this work, the probability distribution ($R(\lambda)$) of uncrimping of the collagen fibers is given by

$$R(\lambda) = \left(\frac{\ln\lambda - \gamma}{\beta}\right)\frac{\alpha}{\beta}\left(\frac{\ln\lambda - \gamma}{\beta}\right)^{\alpha-1}\exp\left(-\left(\frac{\ln\lambda - \gamma}{\beta}\right)^{\alpha}\right) \tag{4}$$

where, α, β and γ are the shape, scale and location parameters with boundary conditions $\alpha, \beta > 0$. The location parameter (γ) when converges to zero modifies Equation (4) to a 2-parameter Weibull Model [29,30]. Moreover, λ_s can be expressed as

$$\lambda_s = e^{\varepsilon_s} \tag{5}$$

Hence, the nominal axial stress P_{zZ} developed in the DCT can be expressed as

$$P_{zZ} = \int_0^{\varepsilon} \alpha\beta^{-\alpha}\,\varepsilon_s^{(\alpha-1)}e^{-\left(\frac{\varepsilon_s}{\beta}\right)^{\alpha}}\left[K(\varepsilon - \varepsilon_s) + \eta\dot{\varepsilon}\right]d\varepsilon_s \tag{6}$$

where, ε and $\dot{\varepsilon}$ represents the experimental failure strain and strain rate. The axial nominal force (F_{zZ}) was calculated as scalar multiplication of physiological cross-sectional area of DCT (A) with the axial nominal stress as shown in Equation (7).

$$F_{zZ} = P_{zZ} * A \tag{7}$$

To normalize the force, a ratio is defined between normal axial force (F_{zZ}) and maximum isometric force (F_{iso}). The force-length curve for the non-linear ligament is further expressed in terms of force ratio (F_r) and stretch ratio (λ) as shown in Equations (8) and (9).

$$F_r = \frac{F_{zZ}}{F_{iso}} \tag{8}$$

$$\lambda = \frac{L}{L_0}; \quad \Delta L = L - L_0 \tag{9}$$

where, L_0 is the resting length and L is the extended length of the DCT. Further, the model accounts for the non-linear material property, finite deformation characteristics, incompressibility of DCTs and anisotropy. A flowchart is provided in Fig. 1 to elucidate the various components involved in the design of the non-linear ligament class.

2.2. GUI for parameter estimation of DCT

In a recently submitted manuscript, the authors of the current work performed experiments on ACL at various strain rates of 0.003, 0.03 and 0.3 s^{-1}. For the sake of reference and convenience, the data is provided in the supplementary section (Supplementary2.xlsx). A polynomial equation of 6th order was curve fitted, and the values of the material parameters were obtained. The coefficient matrix $\bar{p}_{i,j}$ was

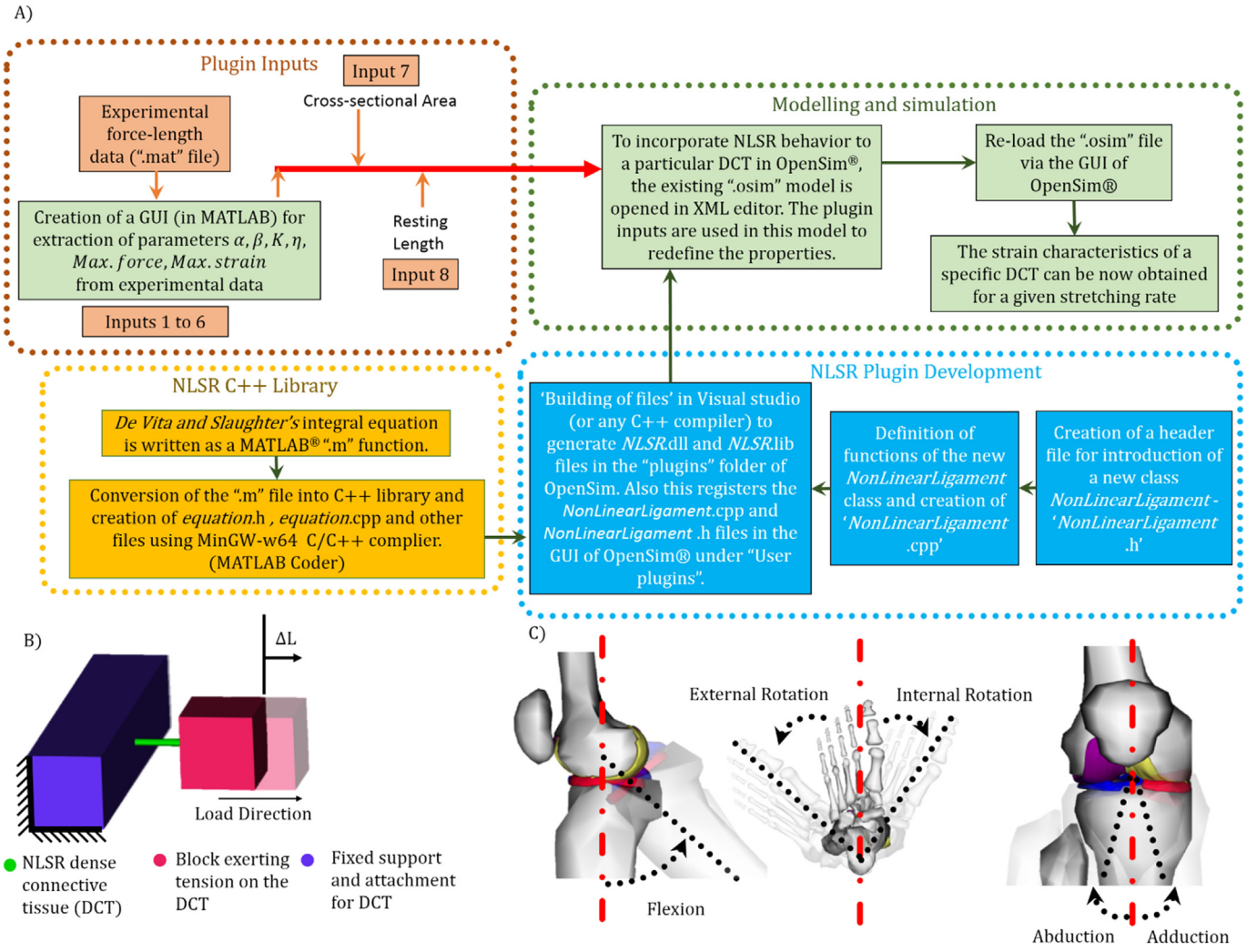

Fig. 1. A) Flow diagram of the non-linear plugin creation; B) tensile simulation of DCTs and C) Flexion, internal rotation, external rotation, adduction and abduction of the knee with 25 DCT bundles.

Table 1
Value for α, β, η and K for DCTs from experimental force-length curve using the GUI.

DCT	Failure strain	Material parameters derived from the experimental data given in the reference column				R^2	Adjusted R^2	Normalized mean	Normalized standard deviation	Reference
		α	β	η (MPa/s)	K (MPa)					
ACL	0.3	4.5	0.3	20	70	0.998	0.998	112.682	147.496	Experimented by the authors. Data given in the supplementary section
						0.997	0.997	121.147	155.386	
						0.714	0.711	205.802	236.316	
PCL	0.21	1.4	0.34	63	600	0.996	0.995	406.795	336.482	[46]
MFL	0.21	1.81	0.12	70	200	0.921	0.919	206.689	170.052	[31]
TL	0.21[a]	1.81[a]	0.12[a]	70[a]	200[a]					
LCL	0.12	1.2	0.2	40	2000	0.810	0.802	224.542	200.560	[52]
PL	0.21	1.1	0.2	65	2500	0.955	0.954	637.027	494.035	[36]
FL	0.21[a]	1.81[a]	0.12[a]	70[a]	200[a]					
CAP	0.29	1.28	0.15	52	180	0.968	0.968	231.181	182.080	[39]
MCL	0.18	1.62	0.3	56	150	0.982	0.981	246.466	204.824	[53]
DMCL	0.06	1.45	0.3	56	1000	0.988	0.987	74.819	69.365	[53]
PT	0.12	1.55	0.3	70	4500	0.989	0.988	897.937	839.361	[19]
lPFL	0.21[a]	1.81[a]	0.12[a]	70[a]	200[a]					
mPFL	0.21[a]	1.81[a]	0.12[a]	70[a]	200[a]					

[a] The failure strain and material parameters are assumed to be the same as MFL.

calculated from the coefficient terms $p_{i,j}$ of each of the samples 'j' as shown in Equation (10) where M and N corresponds to the sample size and the number of coefficients respectively for the 6th order polynomial equation. Regression analysis and estimation of the material parameters were carried out. The material properties for DCTs other than ACL were calculated from the experimental data of frozen-fresh samples as

reported in the literature (refer Table 1). A graphical user interface (GUI) was developed in MATLAB® for the estimation of these material parameters (α, β, η, K, maximum force, maximum strain). The details of the GUI are provided in the supplementary section (Supplementary 2) (Fig. S1).

$$\bar{p}_{i,j} = \frac{\sum_{i=1}^{N} p_{i,j}}{N} \; ; \; j = 1 \; to \; M \tag{10}$$

2.3. Development of the plugin

An open source plugin for OpenSim® platform to predict non-linear behaviour of DCTs at different strain rates was developed based on a structural constitutive model given in Equation (6) [10]. Among the existing structural and phenomenological models, the above-cited model is the only constitutive model that formulates the stress as a function of strain rate ($\dot{\varepsilon}$). The detailed information about the plugin development is provided in the supplementary and the interfaces of the plugin in OpenSim® are provided in the supplementary section.

The developed plugin takes into account of the short-term viscoelastic behaviour of the DCTs with four material parameters viz. α, β, η and K. These parameters are assumed to be identical for the bundles in a DCT i.e. for instance, both anterior ACL (aACL) and posterior ACL (pACL) bundles are assumed identical material parameters [31–33]. The values for material parameters and their corresponding references are provided in Table 1. The force-extension data and cross-sectional area for five DCTs including TL, mPFL, lPFL, aFL and pFL were not available in the literature, therefore the material properties and cross-sectional area of the bundles were assumed to be similar to that of MFL. Further the cross-sectional area of some individual bundles (aPCL, pPCL, cPT, lPT, mPT CAPa, CAPl, CAPo, CAPm, aMCL, iMCL, pMCL, aDMCL and pDMCL) are not available in the literature, and hence it was assumed that the bundles in a given DCT are of equal cross-sectional area to one another as depicted it Table 2.

Table 2
Parameters for defining DCT characteristics.

DCT	Bundles	Resting length (mm)	Cross-sectional area (mm^2)	Max. isometric force (N)	Reference
ACL	aACL	30	20.7	1500	Data given in the supplementary section
	pACL	23.36	19.3	1600	
PCL	aPCL	33.49	21.5	2600	[46]
	pPCL	24.74	21.5		
MFL	aMFL	27.9	7.8	810	[31,37]
	pMFL	31.13	6.7	936.2	
TL[a]	TL	14	7.8	1020	[54–56]
LCL	LCL	69.9	12.22	2000	[52]
PL	PL	46	7.1	1620	[36]
FL[a]	aFL	20	7.8	1034	[21,57]
	pFL	20	7.8	644	
CAP	CAPa	53.5	17.55	1350	[39]
	CAPl	34.5		2000	
	CAPo	60		1500	
	CAPm	34.5		2000	
MCL	aMCL	70	22.47	2500	[41,52,53]
	iMCL	70	22.47	3000	
	pMCL	85.5	22.47	2500	
DMCL	aDMCL	36	31.8	2000	[52,53]
	pDMCL	37	31.8	4500	
PT	mPT	53	16.13	6000	[16,19]
	lPT	53	16.13	6000	
	cPT	48	16.13	6000	
lPFL[a]	lPFL	34	7.8	1159	[58]
mPFL[a]	mPFL	50	7.8	1965	[59–62]

[a] The failure strain and material parameters are assumed to be the same as MFL.

2.4. Simulation for DCTs

A simulation environment to understand the force-extension characteristics of the DCTs were formulated wherein the DCTs were subjected to seven different strain rates from 0.0001 s^{-1} to 100 s^{-1}. The force developed in the tissues were recorded and compared with the existing linear ligament class of OpenSim® by stipulating a motion file for elongation about Z-axis. Fig. 1B illustrates the simulation setup. Furthermore, the literature suggested that the failure time of DCTs during dynamic activities such as running, playing soccer, single leg landing etc. range from 10 to 40 m s [34,35]. Therefore, a simulation of knee joint at the above time frame was conducted for the 13 ligaments, tendons and capsules (corresponding to 25 DCT bundles) namely, anterior cruciate ligament (aACL, pACL), posterior cruciate ligament (aPCL, pPCL), lateral collateral ligament (LCL), medial collateral ligament (aMCL, iMCL, pMCL, aDMCL, pDMCL), popliteofibular ligament (PL), menisco-femoral ligament (aMFL, pMFL), posterior capsules (arcuate popliteal bundle: CAPa, oblique popliteal bundle: CAPo, lateral popliteal bundle: CAPl, medial popliteal bundle: CAPm), medial patellofemoral ligament (mPFL), lateral patellofemoral ligament (lPFL), fibular ligament (aFL, pFL), transverse ligament (TL) and patellar tendons (cPT, mPT, lPT). The prefixes “a”, “p”, “i”, “l”, “m” and “c” signifies anterior, posterior, intermediate, lateral, medial and central respectively. A knee joint model previously published by the authors was used for the simulation. Five kinematics viz. flexion (range from 0° to 120°), internal rotation (IR) (range from 0° to 30°), external rotation (ER) (range from 0° to 40°), adduction (range from 0° to 15°) and abduction (range from 0° to 15°) were simulated for evaluation of force and elongation between 10 and 40 m s. The simulation was carried out using the analysis tool in OpenSim®.

3. Results

The results from tensile testing of fresh cadaveric ACL are given in the supplementary for reference (Supplementary 1). The data was used to calculate the material parameters of ACL as provided in Table 1.

3.1. Parameter estimation

Fig. 2(A) and (B) and (C) illustrates the experimental behaviour of FATC under uniaxial loading at three different strain-rates of 0.003, 0.03 and 0.3 s^{-1}, respectively. The mathematically predicted values of the force-length characteristics are also indicated in the plots. At a given extension, higher strain rate generates higher resistant force in the ligament. Fig. 2(D) to (K) depicts the comparison of the simulated curve with the experimented force-length plots of eight DCT ligaments, tendons and capsules PL, PT, PCL, LCL, CAP, MCL, DMCL and MFL from respective sources. The remaining four DCTs were assumed to have material characteristics similar to MFL. The material parameters calculated through curve-fitting (using the GUI) from the experimental data of the DCTs are tabulated in Table 1. The regression characteristics in terms of R^2 value, adjusted R^2 value, normalized mean and standard deviation for the DCTs are also provided in Table 1. The correlation coefficient ranges from 71.1% to 99.8% with mean value of 92.3% and mean adjusted R-square value of 92.0%.

Fig. 3 depicts the maximum force developed in the 13 DCT ligaments, tendons and capsules (corresponding to 25 DCT bundles) (in logarithmic scale (base 10)) under an extension to their corresponding failure strains. Fig. 4 depicts the force (in kN) and instantaneous strain rate (ISR) (in s^{-1}) developed in few of theDCT bundles of knee during flexion (0°–120°), internal rotation (0°–30°), external rotation (0°–40°), adduction (0°–15°) and abduction (0°–15°) in a time frame of 10 and 40 m s. The individual force-elongation plots at different strain rates are provided in the supplementary section (Figs. S3 to S5) for easy reference. A few DCTs exhibited minimal or no forces during flexion and the plots of force as well as the instantaneous strain rate of these

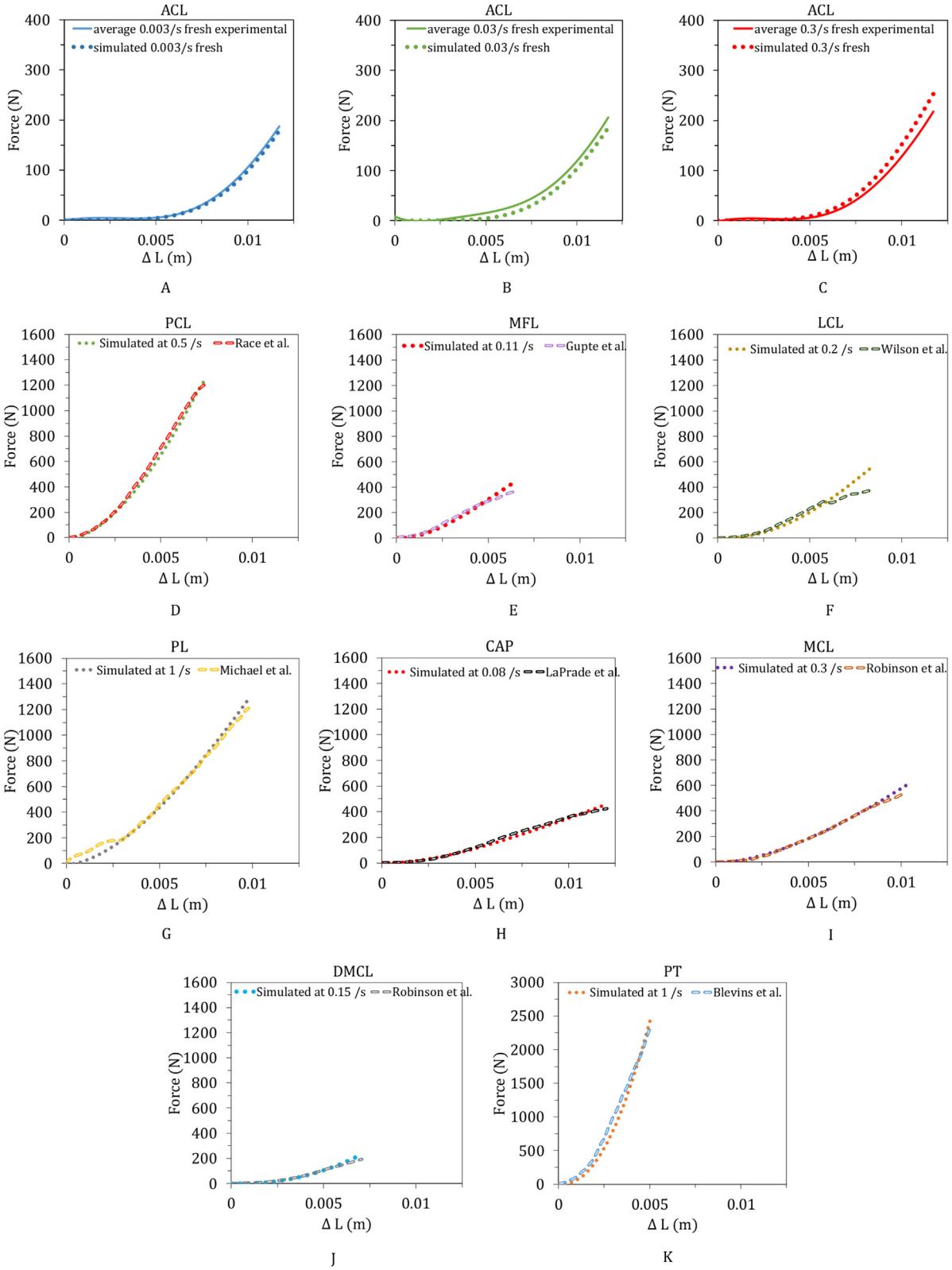

Fig. 2. Input force-length plot for ACL (A, B, C), PCL (D), MFL (E), LCL (F), PL (G), CAP (H), MCL (I), DMCL (J) and PT (K) curve-fitted from literature and experimentation.

bundles are illustrated in Fig. S6 in the supplementary section (Supplementary1.docx). The plots for internal-external rotation and abduction-adduction of all the 25 DCT bundles are given in the supplementary section (Figs. S7 to S10).

4. Discussion

A comparison of maximum force was drawn between the existing class of OpenSim and the developed *NonLinearLigament* class in logarithmic scale (Fig. 3). The existing class of OpenSim was devoid of the

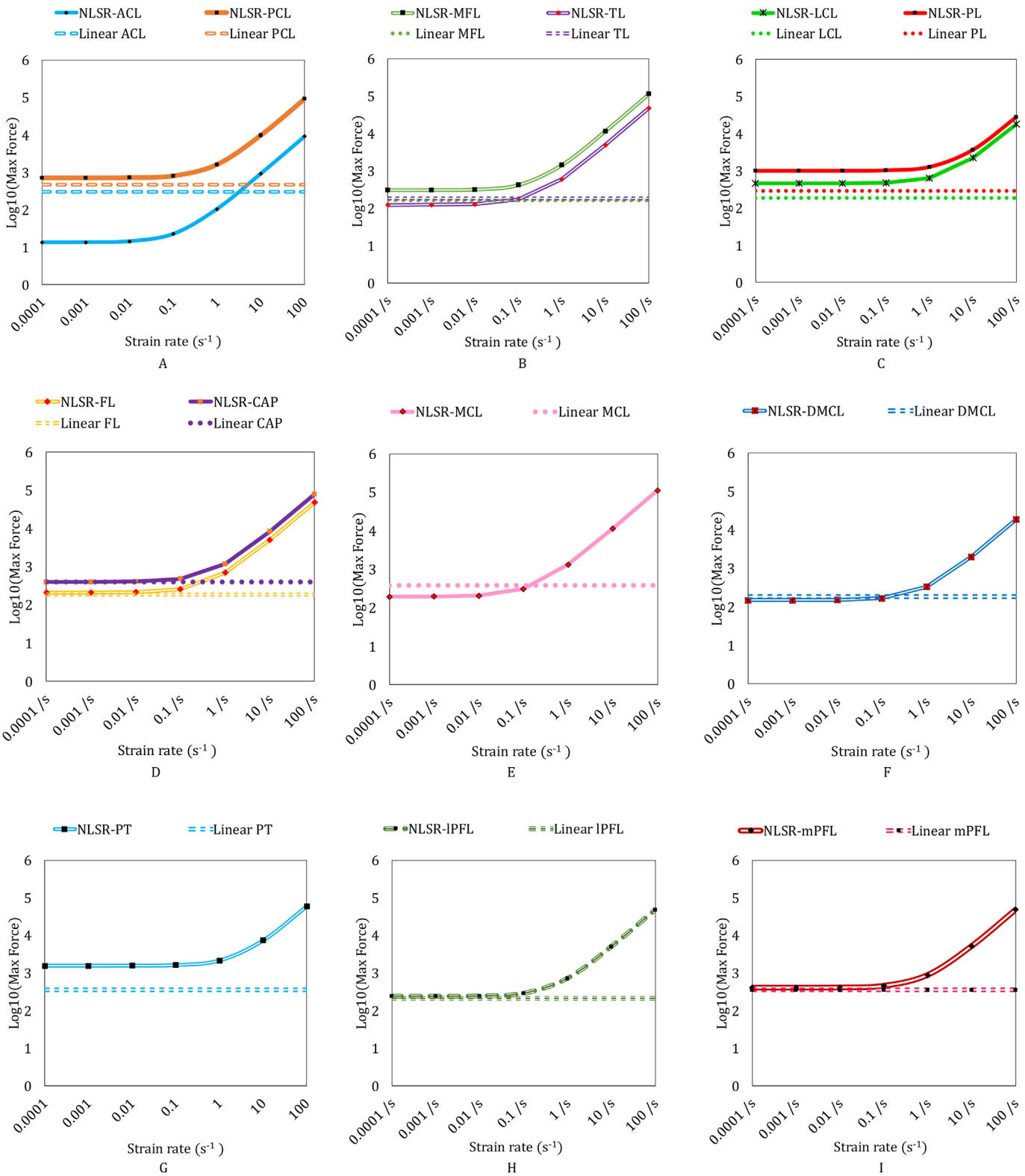

Fig. 3. Logarithmic plot of maximum force generated in NLSR in comparison with linear ligament class of OpenSim® at 0.0001 to 100 s^{-1} strain rates for (A) ACL, PCL (B) MFL, TL (C) LCL, PL (D) FL, CAP (E) MCL (F) DMCL (G) PT (H) lPFL and (I) mPFL.

variation under strain rate i.e. a constant maximum force was observed. However, the proposed class yielded an increase in failure force with an increase in strain rate. The average rate of increase in the maximum force in DCTs from 0.0001 s^{-1} to1 s^{-1} and 1 s^{-1} to 100 s^{-1} are 240.3% and 5904.6% respectively. The maximum increase was evident in ACL with an rate of increase of 688.4% and 8645.1% from 0.0001 s^{-1} to1 s^{-1} and 1 $s^{-1}$to 100 s^{-1}respectively. The minimum rate of increase in the maximum force was evident in PL with 26.5% and 2073.6% from 0.0001 s^{-1} to1 s^{-1} and 1 s^{-1} to 100 s^{-1}respectively.

As most of the DCTs consist of more than one bundle of tissue, further studies on flexion/extension, internal/external rotation and adduction/ abduction were carried out for each of the bundles. The

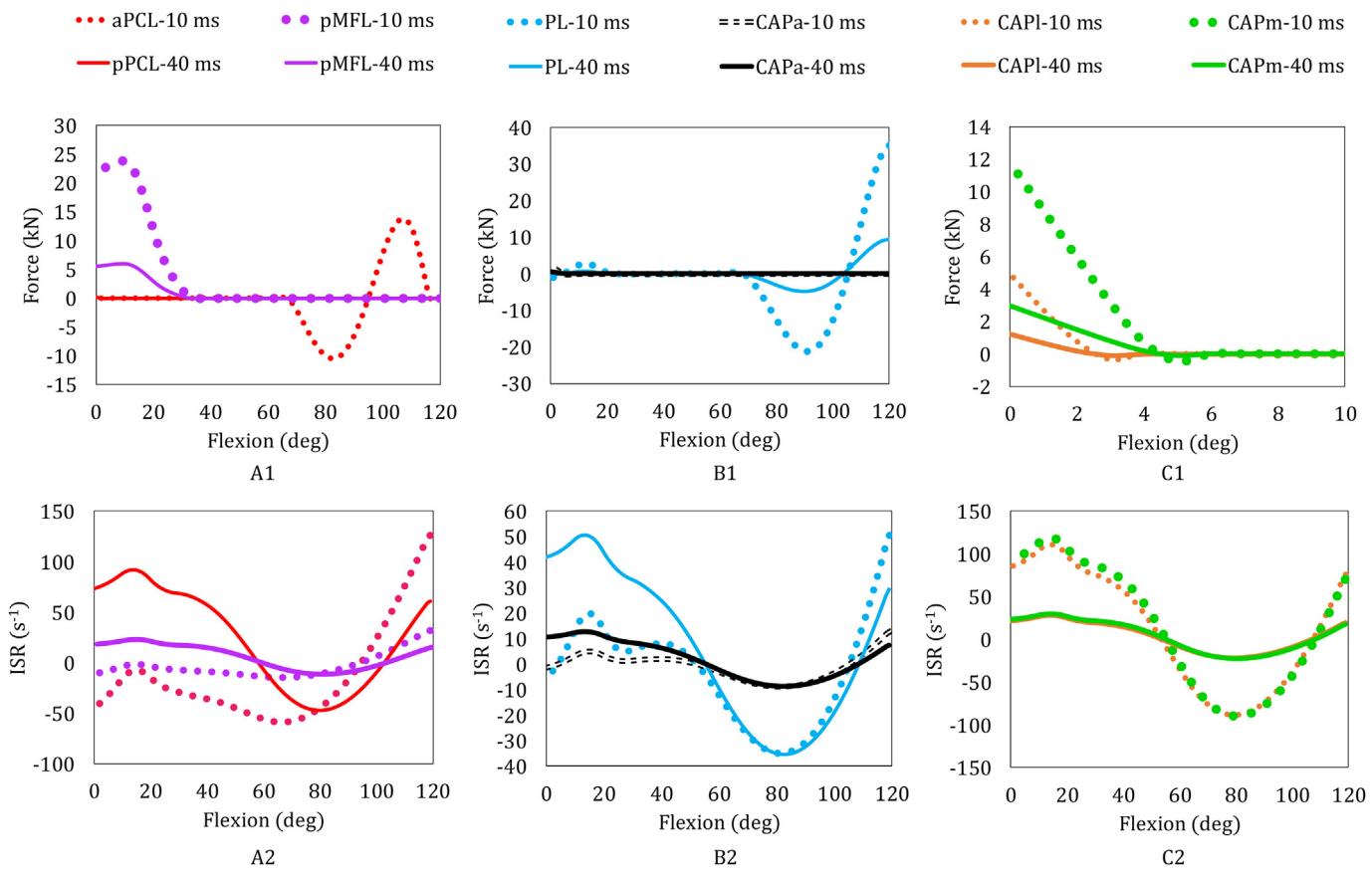

Fig. 4. (A1, B1, C1) Force and (A2, B2, C2) instantaneous strain rate (ISR) plot for (A1, A2) aPCL, pMFL (B1, B2) PL, CAPa and (C1, C2) CAPl, CAPm at different angles of flexion of knee in a time-frame of 10 and 40 ms respectively.

anatomical position of the bundles and their physiology effect the mechanical properties of the bundles at different kinematics. The force and instantaneous strain rate (ISR) (Fig. 4) developed in the prominent DCT bundes under the forward simulation of knee joint for flexion in the time frame of 10 and 40 ms are depicted below. The force and ISR characteristics of flexion (remaining), internal/ external rotation and adduction/ abduction are provided in the supplementary section (Fig. S6 to S10). Table 3 shows the maximum force in the 25 DCT bundles under different knee kinematics. The symbol *N* is indicated for non-significant values of the forces developed in case of few of the DCT bundles.

4.1. Flexion (0°–120°)

The forces developed in aPCL, pMFL, PL, CAPa, CAPl and CAPm (Fig. 4)were higher than the failure force of the corresponding bundles as per literature [36–39] while in the remaining DCT bundles (such as in pACL, aPCL, aMFL, pDMCL etc.) (Supplementary Fig. S6) no significant force was developed owing to the slackness of the bundles as reported in the literature [34,37,40,41].

Anatomically, pMFL attaches to the posterior area of the lateral mensicus and crosses superiorly and medially behind pPCL attaching to the medial condyle of femur [42]. Therefore, the attachment site of these two bundles can be correlated for the high forces and ISRs. PL is anatomically located at the posterio-lateral aspect of the knee making an oblique angle with LCL and connected with the popliteous tendon [43]. During flexion, the obliqueness of the bundles allows it to get stretched along with the popliteous muscle [43]. This justifies the high force and ISR developed in the bundle. CAPa, CAPl and CAPm are located in the posterior aspect of the knee. They also have an attachment at the overlapping point proximal to posterior tibia [16,21,44]. Under flexion, the attachment from the overlapping region and tibia gets stretched and hence high forces and ISR values were observed [17,45]. It was noticed that the ISR plots of all the bundles had a kink at ~30° of flexion. Post 30° of flexion, all the bundles follow a skew asymmetic parabola which is because of the anterior-posterior translation [20,21] of tibia over femur.

4.2. Internal rotation (0°–30°) and external rotation (0°–40°)

When subjected to internal rotation, the forces developed in pPCL, pMFL and CAPm (Supplementary Fig. S7) were higher that the failure forces of the corresponding bundles as per literature [31,39,46] and therefore were prone to failure. pPCL, pMFL and CAPm are connected to the posterio-lateral surface of the medial condyle of femur [21]. During medial rotation, the relative distance between femur and tibia increases in the direction of attachment of the mentioned bundles and therefore, the bundles were strained thereby depicting high forces and ISR. However, the forces generated in the remaining bundles including aACL, pACL, aPCL, aMFL, CAPa, CAPl, CAPo, aMCL, iMCL and pMCL (Supplementary Fig. S7) were within the failure forces of the individual DCTs as per literature [31,39,41,46,47].

During external or lateral rotation, the forces acting on the bundles PL, CAPl, CAPm, aMCL, iMCL and pMCL (Supplementary Fig. S8)were higher in comparison to the maximum failure force of the respective bundles as per literature [36,39,48]. All these bundles excluding PL and CAPl are anatomically attached at the posterior-medial part of the knee [16,21]. Hence during lateral rotation, the bundles were subjected to elongation in the direction of their anatomical attachment resulting in higher forces and ISR value. In the case of PL and CAPl, the bundles underwent elongation in the posterior side during external rotation [16,21]. This results in elevated forces and ISR values. All the bundles

Table 3
Significant forces and ISR of DCT bundles at various kinematics.

DCT Name	Bundles	Flexion		Internal Rotation		External Rotation		Adduction		Abduction	
		@10 m s	@40 m s	@10 m s	@40 m s	@10 m s	@40 m s	@10 m s	@40 m s	@10 m s	@40 m s
ACL	aACL	N		N		N		N		N	
	pACL							1.36[a]	0.348[a]		
								16.6[b]	4.2[b]		
PCL	aPCL	13.76[a]	3.48[a]	N				N			
		125.7[b]	31.42[b]								
	pPCL	N		18.20[a]	5.04[a]					18.9[a]	5.28[a]
				19.8[b]	4.9[b]					19.7 [b]	4.9[b]
MFL	aMFL	N		N						9.89[a]	2.5[a]
										12.9[b]	3.2[b]
	pMFL	23.86[a]	6.01[a]	28[a]	7.58[a]					22.72[a]	6.21[a]
		91.7[b]	22.9[b]	19.90[b]	4.97[b]					16.6[b]	4.2[b]
TL	TL	N		N						N	
LCL	LCL	0.998[a]	0.265[a]					8.9[a]	3.49[a]		
		43.9[b]	11.0[b]					16.7[b]	4.2[b]		
PL	PL	35.12	9.26			49.50[a]	17.22[a]	46.72[a]	17.65[a]		
		50.37[b]	12.6[b]			4.1[b]	−2.0[b]	20.0[b]	5.0[b]		
FL	aFL	N				N		N			
	pFL										
CAP	CAPa	[a] 2.19[a]	[a] 0.55[a]							5.09[a]	1.34[a]
		50.62[b]	12.66[b]							11.5[b]	2.9[b]
	CAPl	4.97[a]	1.24[a]			13.97[a]	3.61[a]	8.89	2.33[a]	N	
		111[b]	27.74[b]			1.5[b]	−0.7[b]	15.2[b]	3.8[b]		
	CAPo	N				N		N			
	CAPm	11.8[a]	2.96[a]	8.3[a]	2.15[a]	16.87[a]	4.35[a]	N		12.96[a]	3.42[a]
		118.4[b]	29.59[b]	16.8[b]	4.2[b]	0.1[b]	0.0[b]			18.6[b]	4.7[b]
MCL	aMCL	N		N		7.98[a]	2.05[a]			14.36[a]	3.71[a]
						2.7[b]	1.3[b]			13.8[b]	3.4[b]
	iMCL					6.992[a]	1.79[a]			13.28[a]	3.43[a]
						2.4[b]	1.2[b]			13.3[b]	3.3[b]
	pMCL					2.53[a]	0.651[a]			6.57[a]	1.69[a]
						2.0[b]	−1.0[b]			10.3[b]	2.6[b]
DMCL	aDMCL					33.76[a]	8.73[a]			18.4[a]	4.8[a]
						7.5[b]	−3.8[b]			26.6[b]	6.7[b]
	pDMCL					22.63[a]	5.87[a]			12.5[a]	3.3[a]
						6.4[b]	−3.2[b]			23.6[b]	5.9[b]
PT	mPT					N				N	
	lPT										
	cPT										
lPFL	lPFL										
mPFL	mPFL										

N- Value not prominent during the simulation (force generated < failure force of the corresponding DCT).
[a] Maximum force developed in the DCT bundle (in kN).
[b] Maximum ISR in the DCT bundle (in s^{-1}).

with significant variations in force were found to have exponentially increasing characteristics of force during both the rotations.

4.3. Adduction (0°–15°) and abduction (0°–15°)

During adduction, the forces generated in the bundles pACL, LCL, PL and CAPl (Supplementary Fig. S9) were found to exceed the failure forces for the corresponding bundles [36,49,50] and therefore were prone to failure. The anatomical attachment sites of pACL, LCL, PL and CAPl are in the lateral condyle of femur and therefore during adduction, these bundles are stretched to the maximum resulting in high forces and ISR values developed in them. However, the forces produced in the other set of bundles such as aACL, aPCL, pPCL, aMFL, CAPa, CAPm, CAPo, aMCL, iMCL and pMCL were below the maximum failure for corresponding DCTs [31,39,41,49,51].

In the process of abduction at the knee, the forces on the bundles pPCL, aMFL, pMFL, CAPa, CAPm, aMCL, pMCL and iMCL (Supplementary Fig. S10) exceed their respective failure forces [34,37,39,41]. The anatomical attachment sites of all the above-mentioned bundles are in the medial condyle of femur and therefore during abduction, these bundles experience maximum elongation compared to the other bundles of knee. This results in development of high forces and ISR values in these bundles and hence they are prone to failure. All other bundles except the ones discussed demonstrated forces below their corresponding failure forces as per literature [11,36,39,40,51].

In summary, the new class of ligament helps in simulating the non-linear behaviour as a function of strain rate. The values of forces obtained during various kinematics are in accordance with the anatomical location of the DCT bundles.

5. Conclusions

A plugin for short-term viscoelasticity of DCT was developed for OpenSim®. The characteristics equation for non-linear strain-rate behaviour was formulated based on four material parameters of the DCT. These material parameters were calculated for DCTs of the knee joint. A simulation was carried out to compare the linear OpenSim® ligament class with the proposed *NLSR* plugin at strain rates varying from 0.0001 s^{-1} to 100 s^{-1}. It was observed that the linear *Ligament* class of OpenSim® was devoid of strain rate dependency and hence was unable to simulate strain rate dependent kinematics for understanding injury mechanics. The *NLSR* plugin created as *NonLinearLigament* class was able to predict the variation in force-length characteristics as a function of strain rates. A simulation of the knee with 25 bundles of DCT was conducted under flexion, IR, ER, adduction and abduction in a time frame of 10 and 40 ms. The following DCT bundles underwent forces

higher than the failure force and hence may fail during the following kinematics:

a) aPCL, pMFL, PL, CAPa, CAPl and CAPm, during flexion
b) pPCL, pMFL and CAPm, during internal rotation
c) pMFL, PL, CAPm, CAPl and aMCL, pMCL and iMCL during external rotation
d) pACL, LCL, PL and CAPl during adduction
e) pPCL, pMFL, CAPa, CAPm and aMCL, pMCL and iMCL during abduction

Hence, it is conclusive that the *NLSR* plugin is capable to simulate strain rate dependent behaviour of DCTs for investigating injuries and failure. However, there are a few limitations of the study. For example, ACL undergoes the highest strains and possible failure during the internal rotation, but the strain values were not captured due to inherent nature of OpenSim® that calculates the strain between the attachment sites and not along the length of the ligament. Further, in real-life injuries, failure may also occur at the site of attachment. In OpenSim® platform, cross-section of the DCT attachment cannot be modelled at this point of time. Future work may consider the above constraints.

Conflicts of interest

This is to declare that none of the authors have any competing interests in the manuscript.

Ethics approval and consent to participate

Not applicable.

Availability of data and material

The data is available with the corresponding author on request.

Consent for publication

We consent for publication of this work.

Funding

The authors would like to acknowledge the funding agencies for their continued support: Indo-German Science and Technology Centre (IGSTC/Call 2014/ Sound4All/24/2015–16), BIRAC, Department of Biotechnology (BIRAC/BT/AIR0275/PACE-12/17), Ministry of Human Resource Development - Design Innovation Centre - IIT Delhi. The funding agencies have no role in the design of the study or the results of the work. No funding has been received for writing assistance.

Authors' contributions

AS developed the plugin and also drafted the early version of the manuscript. DK edited the manuscript.

Acknowledgement

We would like to acknowledge the funding agencies for the support of the work.

Appendix A. Supplementary data

Supplementary data related to this article can be found at https://doi.org/10.1016/j.compbiomed.2019.05.021.

References

[1] G.J. Tortora, B. Derrickson, Principles of Anatomy and Physiology, John Wiley & Sons Inc, 2009.
[2] R. Akoto, M. Balke, J. Höher, K.-H. Frosch, B. Bouillon, C. Lambert, Epidemiology of injuries in judo: a cross-sectional survey of severe injuries based on time loss and reduction in sporting level, Br. J. Sports Med. 52 (17) (2017) 1109–1115.
[3] C.L. Ardern, K.E. Webster, N.F. Taylor, J.A. Feller, Return to sport following anterior cruciate ligament reconstruction surgery: a systematic review and meta-analysis of the state of play, Br. J. Sports Med. 45 (7) (2011) 596–606.
[4] B. Moses, J. Orchard, J. Orchard, Systematic review: annual incidence of ACL injury and surgery in various populations, Res. Sports Med. 20 (3–4) (2012) 157–179.
[5] J.T. Weinhandl, M.C. Hoch, S.Y. Bawab, S.I. Ringleb, Comparison of ACL strain estimated via a data-driven model with in vitro measurements, Comput. Methods Biomech. Biomed. Eng. 19 (14) (2016) 1550–1556.
[6] R.F. Escamilla, T.D. Macleod, K.E. Wilk, L. Paulos, J.R. Andrews, ACL strain and tensile forces for weight bearing and non—weight-bearing exercises after ACL reconstruction: a guide to exercise selection, J. Orthop. Sport. Phys. Ther. 42 (3) (2012) 208–220.
[7] E. Roldán, N.D. Reeves, G. Cooper, K. Andrews, Design consideration for ACL implants based on mechanical loading, Procedia CIRP 49 (2016) 133–138.
[8] A. Bijalwan, B.P. Patel, M. Marieswaran, D. Kalyanasundaram, Volumetric locking free 3D finite element for modelling of anisotropic visco-hyperelastic behaviour of anterior cruciate ligament, J. Biomech. 73 (2018) 1–8.
[9] D.B. Burr, C. Milgrom, D. Fyhrie, M. Forwood, M. Nyska, A. Finestone, S. Hoshaw, E. Saiag, A. Simkin, In vivo measurement of human tibial strains during vigorous activity, Bone 18 (5) (1996) 405–410.
[10] R. De Vita, W.S. Slaughter, A structural constitutive model for the strain rate-dependent behavior of anterior cruciate ligaments, Int. J. Solids Struct. 43 (6) (2006) 1561–1570.
[11] T.J. Bonner, N. Newell, A. Karunaratne, A.D. Pullen, A.A. Amis, M.J.A. Bull, S.D. Masouros, Strain-rate sensitivity of the lateral collateral ligament of the knee, J. Mech. Behav. Biomed. Mater. 41 (2015) 261–270.
[12] G. Li, J. Gil, A. Kanamori, S.-Y.L. Woo, A validated three-dimensional computational model of a human knee joint, J. Biomech. Eng. 121 (6) (1999) 657–662.
[13] A. Kiapour, A.M. Kiapour, V. Kaul, C.E. Quatman, S.C. Wordeman, T.E. Hewett, C.K. Demetropoulos, V.K. Goel, Finite element model of the knee for investigation of injury mechanisms: development and validation, J. Biomech. Eng. 136 (1) (2014) 11002.
[14] M.G. Pandy, K. Sasaki, S. Kim, A three-dimensional musculoskeletal model of the human knee joint. Part 1: theoretical construction, Comput. Methods Biomech. Biomed. Eng. 1 (2) (1997) 87–108.
[15] A.J. Van Den Bogert, T. Geijtenbeek, O. Even-Zohar, F. Steenbrink, E.C. Hardin, A real-time system for biomechanical analysis of human movement and muscle function, Med. Biol. Eng. Comput. 51 (10) (2013) 1069–1077.
[16] A. Schmitz, D. Piovesan, Development of an open-source, discrete element knee model, IEEE Trans. Biomed. Eng. 63 (10) (2016) 2056–2067.
[17] A. Schmitz, D. Piovesan, Development of an open-source cosimulation method of the knee, 2016 38th Annual International Conference of the IEEE Engineering in Medicine and Biology Society (EMBC), IEEE, 2016, pp. 6034–6037.
[18] J.P. Fisk, J.S. Wayne, Development and validation of a computational musculoskeletal model of the elbow and forearm, Ann. Biomed. Eng. 37 (4) (2009) 803–812.
[19] F.T. Blevins, A.T. Hecker, G.T. Bigler, A.L. Boland, W.C. Hayes, The effect of donor age and strain rate on the biomechanical properties of bone-patellar tendon-bone allografts, Am. J. Sports Med. 22 (3) (1994) 328–333.
[20] H. Xu, D. Bloswick, A. Merryweather, An improved OpenSim gait model with multiple degrees of freedom knee joint and knee ligaments, Comput. Methods Biomech. Biomed. Eng. 18 (11) (2015) 1217–1224.
[21] M. Marieswaran, A. Sikidar, A. Goel, D. Joshi, D. Kalyanasundaram, An extended OpenSim knee model for analysis of strains of connective tissues, Biomed. Eng. Online 17 (1) (2018) 42.
[22] D.P. Pioletti, L.R. Rakotomanana, J.-F. Benvenuti, P.-F. Leyvraz, Viscoelastic constitutive law in large deformations, J. Biomech. 31 (8) (1998) 753–757.
[23] H. Koga, T. Muneta, ACL injury mechanisms, in: M. Ochi, K. Shino, K. Yasuda, M. Kurosaka (Eds.), ACL Injury and its Treatment, Springer, Japan, Tokyo, 2016, pp. 113–125.
[24] R. Sopakayang, R. De Vita, A mathematical model for creep, relaxation and strain stiffening in parallel-fibered collagenous tissues, Med. Eng. Phys. 33 (9) (2011) 1056–1063.
[25] N. Sasaki, S. Odajima, Elongation mechanism of collagen fibrils and force-strain relations of tendon at each level of structural hierarchy, J. Biomech. 29 (9) (1996) 1131–1136.
[26] A. Sverdlik, Y. Lanir, Time-dependent mechanical behavior of sheep digital tendons, including the effects of preconditioning, J. Biomech. Eng. 124 (1) (2002) 78.
[27] M.S. Sacks, Incorporation of experimentally-derived fiber orientation into a structural constitutive model for planar collagenous tissues, J. Biomech. Eng. 125 (2) (2003) 280.
[28] J.E. Bischoff, Continuous versus discrete (invariant) representations of fibrous structure for modeling non-linear anisotropic soft tissue behavior, Int. J. Non-Linear Mech. 41 (2) (2006) 167–179.
[29] B. Loret, Biomechanical Aspects of Soft Tissues, CRC Press, Boca Raton , 2017 Taylor & Francis, 2017.
[30] C. Hurschler, P.P. Provenzano, R. Vanderby, Application of a probabilistic microstructural model to determine reference length and toe-to-linear region transition in

fibrous connective tissue, J. Biomech. Eng. 125 (3) (2003) 415.
[31] C.M. Gupte, A. Smith, N. Jamieson, A.M.J. Bull, R.D.W. Thomas, A.A. Amis, Meniscofemoral ligaments - structural and material properties, J. Biomech. 35 (12) (2002) 1623–1629.
[32] K.F. Mallett, E.M. Arruda, Digital image correlation-aided mechanical characterization of the anteromedial and posterolateral bundles of the anterior cruciate ligament, Acta Biomater. 56 (2017) 44–57.
[33] S.G. McLean, K.F. Mallett, E.M. Arruda, Deconstructing the anterior cruciate ligament: what we know and do not know about function, material properties, and injury mechanics, J. Biomech. Eng. 137 (2) (2015) 020906.
[34] M.S. Schulz, K. Russe, A. Weiler, H.J. Eichhorn, H.J. Strobel, Epidemiology of posterior cruciate ligament injuries, Arch. Orthop. Trauma Surg. 123 (4) (2003) 186–191.
[35] H. Koga, T. Muneta, ACL injury mechanisms, ACL Injury and its Treatment, Springer, Japan, Tokyo, 2016, pp. 113–125.
[36] M.J. Maynard, Xianghua Deng, T.L. Wickiewicz, R.F. Warren, The popliteofibular ligament, Am. J. Sports Med. 24 (3) (1996) 311–316.
[37] a R. Poynton, S.M. Javadpour, P.J. Finegan, M. O'Brien, The meniscofemoral ligaments of the knee, J. Bone Jt. Surg. Br. 79 (2) (1997) 327–330.
[38] A.A. Amis, C.M. Gupte, A.M.J. Bull, A. Edwards, Anatomy of the posterior cruciate ligament and the meniscofemoral ligaments, Knee Surg. Sport. Traumatol. Arthrosc. 14 (3) (2006) 257–263.
[39] R.F. LaPrade, P.M. Morgan, F.A. Wentorf, S. Johansen, L. Engebretsen, The anatomy of the posterior aspect of the knee: an anatomic study, J. Bone Jt. Surg. Ser. A 89 (4) (2007) 758–764.
[40] M. Marieswaran, I. Jain, B. Garg, V. Sharma, D. Kalyanasundaram, A review on biomechanics of anterior cruciate ligament and materials for reconstruction, Appl. Bionics Biomechanics (2018) 1–14 2018.
[41] F. Liu, B. Yue, H.R. Gadikota, M. Kozanek, W. Liu, T.J. Gill, H.E. Rubash, G. Li, Morphology of the medial collateral ligament of the knee, J. Orthop. Surg. Res. 5 (1) (2010) 1–8.
[42] T. Kusayama, C.D. Harner, G.J. Carlin, J.W. Xerogeanes, B.A. Smith, Anatomical and biomechanical characteristics of human meniscofemoral ligaments, Knee Surg. Sport. Traumatol. Arthrosc. 2 (4) (1994) 234–237.
[43] S.P. Jadhav, S.R. More, R.F. Riascos, D.F. Lemos, L.E. Swischuk, Comprehensive review of the anatomy, function, and imaging of the popliteus and associated pathologic conditions, Radiographics 34 (2) (2014) 496–513.
[44] M.G. PANDY, K. SASAKI, S. KIM, A three-dimensional musculoskeletal model of the human knee joint. Part 1: theoretical construction, Comput. Methods Biomech. Biomed. Eng. 1 (2) (1997) 87–108.
[45] K.B. Shelburne, H.J. Kim, W.I. Sterett, M.G. Pandy, Effect of posterior tibial slope on knee biomechanics during functional activity, J. Orthop. Res. 29 (2) (2011) 223–231.
[46] A. Race, A.A. Amis, The mechanical properties of the two bundles of the human posterior cruciate ligament, J. Biomech. 27 (1) (1994) 13–24.
[47] M. Marieswaran, N. Mansoori, V.K. Digge, S.K. Jhajhria, Effect of Preservation Methods on Tensile Properties of Human Femur- ACL-Tibial Complex (FATC) – A Cadaveric Study on Male Subjects, (2018), pp. 1–28.
[48] C.B. Frank, Ligament structure, physiology and function, J. Musculoskelet. Neuronal Interact. 4 (2) (2004) 199–201.
[49] B. Dai, M. Mao, W.E. Garrett, B. Yu, Biomechanical characteristics of an anterior cruciate ligament injury in javelin throwing, J. Sport Heal. Sci. 4 (4) (2015) 333–340.
[50] R.F. LaPrade, T.V. Ly, F.A. Wentorf, L. Engebretsen, The posterolateral attachments of the knee: a qualitative and quantitative morphologic analysis of the fibular collateral ligament, popliteus tendon, popliteofibular ligament, and lateral gastrocnemius tendon, Am. J. Sports Med. 31 (6) (2003) 854–860.
[51] K.F. Bowman, J.K. Sekiya, Anatomy and biomechanics of the posterior cruciate ligament, medial and lateral sides of the knee, Sports Med. Arthrosc. 18 (4) (2010) 222–229.
[52] W.T. Wilson, A.H. Deakin, A.P. Payne, F. Picard, S.C. Wearing, Comparative analysis of the structural properties of the collateral ligaments of the human knee, J. Orthop. Sport. Phys. Ther. 42 (4) (2012) 345–351.
[53] J.R. Robinson, A.M.J. Bull, A.A. Amis, Structural properties of the medial collateral ligament complex of the human knee, J. Biomech. 38 (5) (2005) 1067–1074.
[54] M. Faruch-Bilfeld, F. Lapegue, H. Chiavassa, N. Sans, Imaging of meniscus and ligament injuries of the knee, Diagn. Interv. Imaging 97 (7–8) (2016) 749–765.
[55] M. Bv, N. Narga, K. Ashwin, M. Mp, K. Naveen, G. Chandni, R. Biswabina, C. Gk, Original Research Article the Anterior Transverse Ligament of Knee : Morphological Morphometric Study in Formalin Fixed Human Fetuses and Department of Anatomy, Manipal University , Melaka Manipal Medical College (Manipal Campus), 2014, pp. 24–28.
[56] C. Muhle, W.O. Thompson, R. Sciulli, R. Pedowitz, J.M. Ahn, L. Yeh, P. Clopton, P. Haghighi, D.J. Trudell, D. Resnick, Transverse ligament and its effect on meniscal motion. Correlation of kinematic MR imaging and anatomic sections, Investig. Radiol. 34 (9) (1999) 558–565.
[57] T. Sugita, A.A. Amis, Anatomic and biomechanical study of the lateral collateral and popliteofibular ligaments, Am. J. Sports Med. 29 (4) (2001) 466–472.
[58] S. Capkin, G. Zeybek, I. Ergur, C. Kosay, A. Kiray, An anatomic study of the lateral patellofemoral ligament, Acta Orthop. Traumatol. Turcica 51 (1) (2017) 73–76.
[59] J. Mountney, W. Senavongse, A.A. Amis, N.P. Thomas, Tensile strength of the medial patellofemoral ligament before and after repair or reconstruction, J. Bone Jt. Surg. Br. 87 (1) (2005) 36–40.
[60] A.A. Amis, P. Firer, J. Mountney, W. Senavongse, N.P. Thomas, Anatomy and biomechanics of the medial patellofemoral ligament, The Knee 10 (3) (2003) 215–220.
[61] R. Philippot, J. Chouteau, J. Wegrzyn, R. Testa, M.H. Fessy, B. Moyen, Medial patellofemoral ligament anatomy: implications for its surgical reconstruction, Knee Surg. Sport. Traumatol. Arthrosc. 17 (5) (2009) 475–479.
[62] V. De Oliveira, V. De Souza, R. Cury, O.P. Camargo, O. Avanzi, N. Severino, P. Fucs, Medial patellofemoral ligament anatomy: is it a predisposing factor for lateral patellar dislocation? Int. Orthop. 38 (8) (2014) 1633–1639.